# Fronts and pulses in an enzymatic reaction catalyzed by glucose oxidase

**David G. Míguez*†, Vladimir K. Vanag†, and Irving R. Epstein†**

Department of Chemistry and Volen Center for Complex Systems, MS 015, Brandeis University, Waltham, MA 02454

Edited by Kenneth Showalter, West Virginia University, Morgantown, WV, and accepted by the Editorial Board February 23, 2007 (received for review December 21, 2006).

**Waves and patterns in living systems are often driven by biochemical reactions with enzymes as catalysts and regulators. We present a reaction–diffusion system catalyzed by the enzyme glucose oxidase that exhibits traveling wave patterns in a spatially extended medium. Fronts and pulses propagate as a result of the coupling between the enzyme-catalyzed autocatalytic production and diffusion of hydrogen ions. A mathematical model qualitatively explains the experimental observations.**

enzymes | reaction–diffusion | waves

Cardiac muscle waves (1), calcium waves in cells (2), glycolytic waves (3, 4), metabolic waves in neutrophils (5, 6), and other biological waves have been the subject of many investigations because of their importance in living systems. Waves in biological systems have inspired many studies of chemical waves in the spatially extended Belousov–Zhabotinsky reaction (7). Despite the fact that biological and chemical waves occur in very different media, they share several features in common. Some of these phenomena can be described by quite general equations, like the Fisher–Kolmogorov result (8, 9) for the velocity of front propagation

$$V = 2(Dk[\mathrm{S}])^{1/2}, \qquad [1]$$

where $D$ is the diffusion coefficient of an autocatalytic species (activator X) generated with rate constant $k$ in a reaction schematically represented as Eq. **2**:

$$\mathrm{S} + \mathrm{X} \rightarrow 2\mathrm{X}. \qquad [2]$$

Fronts, waves, and patterns have been investigated not only in the Belousov–Zhabotinsky reaction and the much richer Belousov–Zhabotinsky–AOT systems (10, 11), but also in many other chemical reactions, including pH oscillators (12, 13) that operate under softer, more biologically compatible conditions (e.g., without strong acid).

Despite the considerable progress made in characterizing and understanding chemical and biological waves and patterns in the past several decades, there remains a significant gap between these two types of waves, namely that there has been no clear experimental demonstration of fronts or waves in simple, controllable, artificial enzymatic systems containing one or a few enzymes (we exclude complex natural systems like glycolysis).

There are many advantages of a pattern formation system based on enzymatic reactions. Substrate specificity reduces cross-reactions between chemical species, facilitating the design and modeling of new bifurcating enzymatic systems. By using well developed biochemical or bioengineering techniques, enzymes can be immobilized on various surfaces, as well as in gels and microspheres, allowing the possibility of developing small biochemical devices that use the principles of nonlinear science. Combining nonlinear (autocatalytic, bistable, oscillatory, etc.) enzymatic reactions with enzyme immobilization in spatially extended systems opens up the possibility of using nonlinear biochemical systems to produce complex patterns inaccessible with nonlinear systems based on inorganic chemistry. Waves and pulses in simple, artificially designed enzymatic systems may shed new light on natural waves and patterns in biological systems.

We have previously studied the temporal dynamics of the enzymatic autocatalytic reaction between glucose and ferricyanide ($\mathrm{F_i}$), catalyzed by the enzyme glucose (G) oxidase (GO) in a continuously stirred tank reactor (CSTR), where the addition of negative feedback can induce oscillatory behavior (14). In this paper, we present spatial patterns (waves and pulses) in this biochemical system.

GO (EC 1.1.3.4, from the mold *Aspergillus niger*) (15–17) is a well known flavin-containing glycoprotein that catalyzes the oxidation of D-G in the presence of a variety of oxidizing substances (oxygen, $\mathrm{F_i}$, and many others). With $\mathrm{F_i}$ as substrate, the "ping-pong" mechanism (18) for GO can be written as

$$\mathrm{E_{ox}} + \mathrm{G} \rightarrow \mathrm{E_r} + \mathrm{P}, \qquad [3]$$

$$\mathrm{E_r} + \mathrm{F_i} \rightarrow \mathrm{E_s} + \mathrm{F_e} + \mathrm{H^+}, \qquad [4]$$

and

$$\mathrm{E_s} + \mathrm{F_i} \rightarrow \mathrm{E_{ox}} + \mathrm{F_e} + \mathrm{H^+}, \qquad [5]$$

where $\mathrm{E_{ox}}$, $\mathrm{E_s}$, and $\mathrm{E_r}$ represent GO with the active center, flavin adenine dinucleotide, in its oxidized, semiquinone, and reduced forms, respectively, and $\mathrm{F_e}$ is ferrocyanide. Under our experimental conditions, where the concentrations of G and $\mathrm{F_i}$ are above and below, respectively, their Michaelis constants, the total rate ($v_e$) of Eqs. **3–5** can be written as

$$v_e = k_{ox}[\mathrm{F_i}]e_t, \qquad [6]$$

where $e_t$ is the total concentration of all forms of GO and $k_{ox}$ is a pH-dependent rate constant corresponding to the sum of Eqs. **4** and **5** (14, 17, 19):

$$k_{ox} = [\mathrm{H^+}](k_1K_e^2 + k_2[\mathrm{H^+}]^2)/(K_e^2 + [\mathrm{H^+}]^2). \qquad [7]$$

In the pH range 3–7, where all our processes take place, $k_2 \gg k_1$ and $K_e \cong 10^{-4}$ M. The constant $k_1$ ($k_2$) is the major determinant of $k_{ox}$ at pH $> 4$ ($3 <$ pH $< 4$). Because hydrogen

Author contributions: D.G.M. and V.K.V. designed research; D.G.M. and V.K.V. performed research; D.G.M., V.K.V., and I.R.E. analyzed data; and D.G.M., V.K.V., and I.R.E. wrote the paper.

The authors declare no conflict of interest.

This article is a PNAS Direct Submission. K.S. is a guest editor invited by the Editorial Board.

Abbreviations: G, glucose; GO, G oxidase; $\mathrm{F_i}$, ferricyanide; $\mathrm{F_e}$, ferrocyanide; CSTR, continuously stirred tank reactor; CFUR, continuously fed unstirred reactor; SS, steady state; PDE, partial differential equation.

*Present address: Department of Systems Biology, Harvard Medical School, Boston, MA 02115.

†To whom correspondence may be addressed. E-mail: david_miguez@hms.harvard.edu, vanag@brandeis.edu, or epstein@brandeis.edu.

This article contains supporting information online at www.pnas.org/cgi/content/full/0611438104/DC1.





www.pnas.org/cgi/doi/10.1073/pnas.0611438104

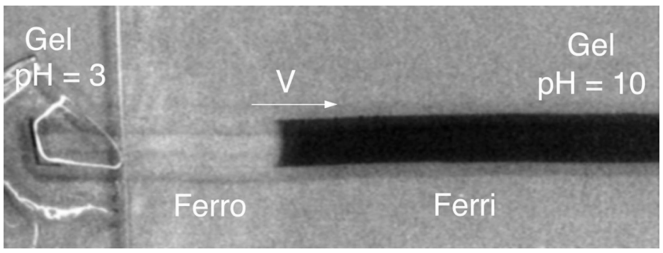


**Fig. 1.** Snapshot of front propagation in batch conditions in a gel layer. Front moves in the direction of the arrow. In the gel, [GO] = 0.3 mg/ml, [$F_i$] = 15 mM, and [G] = 100 mM.

ions are produced in Eqs. **4** and **5** and $k_{ox}$ increases with $[H^+]$, the overall enzymatic reaction is autocatalytic (14). We can write the rate as

$$\partial[H^+]/\partial t = k_{ox}'[H^+][F_i]e_t, \qquad [8]$$

where $k'_{ox} = k_{ox}/[H^+]$; $k'_{ox} \cong k_1$ at pH > p$K_e$ and $k'_{ox} \cong k_2$ at pH < p$K_e$. In experiments in a stirred cell, this autocatalysis leads to an accelerating decrease in pH, from an initial value of 6–8 to a final pH of 3.2–3.5. From the general theory of waves and fronts (see, e.g., ref. 20 or 21), it follows that Eqs. **3–5** can generate a front propagating with constant velocity in a spatially extended system.

If we introduce a back reaction that restores the product, $F_e$, to its initial form, $F_i$, while appropriately reducing the concentration of protons, it should be possible to produce a pulse of hydrogen ions. For this purpose, we choose the reaction between hydrogen peroxide and $F_e$ (22).

$$H_2O_2 + 2F_e + 2H^+ \rightarrow 2F_i + 2H_2O. \qquad [9]$$

We report here experiments in which the autocatalytic Eqs. **3–5** with GO immobilized in a polyacrylamide gel generate fronts. Addition of negative feedback in the form of Eq. **9** can transform the front into a pulse under appropriate conditions. Fronts and pulses both propagate with constant velocity. We also simulate the experimental results with a simple mechanism that clarifies some of our experimental observations.

## Results

**Experimental Fronts.** In batch conditions and without the addition of $H_2O_2$, our system is unstable at nonzero concentrations of $F_i$ because of the autocatalytic Eqs. **3–5.** However, at high pH (>6–7), the system can be considered as "quasistable" for short periods, because autocatalysis is then slow. An initial perturbation imposed at one end of a slice of gel, which puts a portion of the system into its final, stable, low pH (pH 3) state, travels through the gel as a front propagating into an unstable state (see refs. 23–26 for theoretical studies of such systems). Fig. 1 presents a snapshot of a typical experiment. The front moves by consuming $F_i$ (dark region), producing hydrogen ion and $F_e$ (lighter region).

We examined the dependence of the front velocity $v$ on the initial concentrations of $F_i$, [$F_i$] ($\equiv s_0$), and [GO] ($\equiv e_t$) to test Eq. **1** for our system, where the effective rate constant $k$ in Eq. **1** is given by $k'_{ox}s_0e_t$ (see Eq. **8**), and $k'_{ox}$ depends on pH according to Eq. **7**. Fig. 2*a* and curve 1 in Fig. 2*c* present typical experimental results. We see that $v$ increases linearly with both $s_0^{1/2}$ and $e_t^{1/2}$, as predicted by Eq. **1**. However, extrapolation of the trend lines for the three different values of $e_t$ (Fig. 2*a*) shows that the velocity of the front goes to zero at a nonzero $s_0$, in contradiction to Eq. **1**. We were not able to test this prediction experimentally, because the contrast for such small values of [$F_i$] was so low that the front could not be distinguished. We consider this behavior

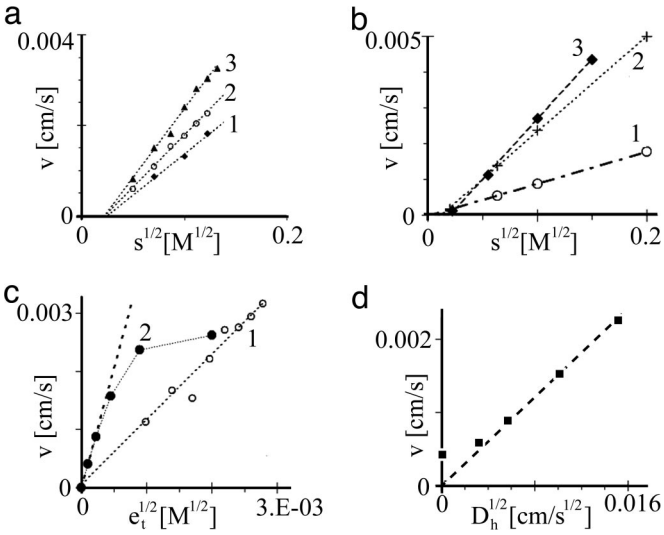


**Fig. 2.** Dependence of the front velocity $v$ on $[F_i]^{1/2}$ (*a* and *b*), $e_t^{1/2}$ (*c*), and $D_h^{1/2}$ (*d*). (*a*) Experimental results. [GO] = 0.15 mg/ml (curve 1), 0.3 mg/ml (curve 2), and 0.6 mg/ml (curve 3), and [G] = 100 mM. (*b*) Numerical simulations for Eqs. **3-5** and **10** and **11**. $e_t = 5 \times 10^{-8}$ M (curve 1), $8 \times 10^{-7}$ M (curve 2), and $2 \times 10^{-6}$ M (curve 3). $k_1 = 3.5 \times 10^6$ $M^{-2}{\cdot}s^{-1}$, $k_2 = 3.0 \times 10^7$ $M^{-2}{\cdot}s^{-1}$, $K_e = 10^{-4}$ M (p$K_e$ = 4), p$K_G$ = 4.6, p$K_F$ = 3.6, $N_{AG}$ = 200, and $k_b = 10^9$ $M^{-1}{\cdot}s^{-1}$. $D_h = 3 \times 10^{-5}$ $cm^2/s$ and $D_s = D_p = D_{ph} = 10^{-5}$ $cm^2{\cdot}s^{-1}$. Initial pH = 7–8 ($v$ is nearly independent of initial pH). (*c*) Curve 1 shows the experimental results for $s_0$ = 8.75 mM and [G] = 100 mM with an initial pH = 10. Curve 2 shows the numerical simulation for $D_h = 3 \times 10^{-5}$ $cm^2{\cdot}s^{-1}$ and $s_0$ = 10 mM. (*d*) Numerical simulations for $s_0 = 10^{-2}$ M and $e_t = 5 \times 10^{-8}$ M; all other parameters were as described for *b*.

theoretically in the next section. The slopes of curves 1–3 in Fig. 2*a* divided by corresponding values of $(e_t)^{1/2}$ and the slope of curve 1 in Fig. 2*c* divided by $s_0^{1/2}$ provide us with information about the value of $2(D_hk'_{ox})^{1/2}$, which we calculate as 12–16 $cm{\cdot}s^{-1}{\cdot}M^{-1}$. Knowing $k'_{ox}$ in a gel (which can differ from $k'_{ox}$ measured in a CSTR and which depends on pH), we can estimate $D_h$, the diffusion coefficient of hydrogen ion in the gel.

Experiments at several initial pHs show that the velocity of the front is almost independent of the pH, in agreement with Eq. **1**. Changes of five orders of magnitude in the concentration of protons (from pH 10 to pH 5) produce an increase of the front velocity of only about a factor of two [see supporting information (SI) Figs. 5 and 6 and *SI Results*].

In experiments on another bistable chemical reaction, the $F_e$-iodate- sulfite system in a continuously fed unstirred reactor (CFUR), two approaching pH fronts did not collide but stopped when the distance between them became sufficiently small (0.5 mm) (12). We studied the interaction of fronts in our enzymatic system at several reactant concentrations. When the reaction is conducted in a CFUR, the tank reactor acts not only as a supplier of fresh reactants but also as a sink for products, removing them from the gel. In a sense, the feeding chamber provides a negative feedback similar to the role played by Eq. **9**, which removes $H^+$ and supplies the substrate, $F_i$. The major difference between this "diffusion-modulated" feedback and a chemical feedback like Eq. **9** is that the strength of the diffusion-modulated feedback depends on the thickness of the layer as $\tau \cong l^2/D$, where $\tau$ is the characteristic time for a molecule to diffuse across the thickness of the layer, $l$. Notice that the term "layer" should include gel layer and membranes separating the gel from the feeding chamber. The concentrations of reactants in the feeding chamber ($F_i$ and $OH^-$ in our case) and $l$ are the key parameters that determine the state of the system in the gel layer (27, 28), which

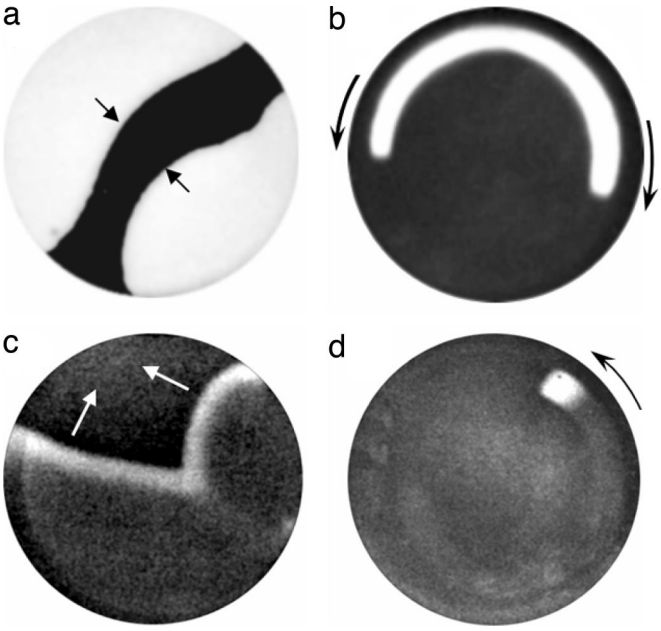


**Fig. 3.** Snapshots of experimentally observed fronts (*a* and *b*) and pulses (*c* and *d*) in a CFUR with 2D (*a* and *c*) and quasi-1D (*b* and *d*) geometry. Concentration of immobilized GO in the entire gel (*a* and *c*) or in the annular stripe (*b* and *d*) is 0.3 mg/ml. The concentrations in the feeding chamber were [G] = 100 mM, pH 10 (adjusted with NaOH); [$F_i$] = 20 mM (*a*), 10 mM (*b*), and 15 mM (*c* and *d*); and [$H_2O_2$] = 0 mM (*a* and *b*) and 20 mM (*c* and *d*). The diameter of each circular gel layer is 25.4 mm. Arrows denote the directions of front or pulse propagation.

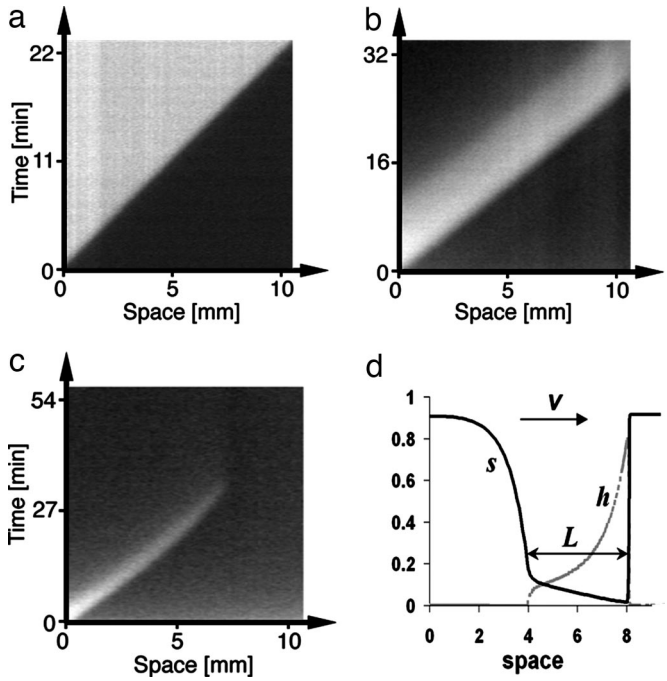


**Fig. 4.** Spatiotemporal behavior of fronts and pulses in a CFUR. (*a–c*) Space–time plots for front and pulse patterns in a CFUR at [$F_i$] = 15 mM, [G] = 100 mM, and pH 10 in the feeding chamber and 0.3 mg/ml immobilized GO in the gel. (*a*) Front; [$H_2O_2$] = 10 mM. (*b*) Pulse; [$H_2O_2$] = 20 mM. (*c*) Damped pulse; [$H_2O_2$] = 30 mM. The slopes of the space–time plots give velocities of 0.47, 0.43, and 0.22 mm/min for the front (*a*), pulse (*b*), and damped pulse (*c*), respectively. (*d*) Shape of a pulse in the model represented by Eqs. **17** and **18** with parameters $\alpha = 0.0121$, $\beta = \gamma = 10^{-5}$, $R = 0.81$, $D_s = 2.5 \times 10^{-5}$, $D_h = 5 \times 10^{-5}$, $v = 0.0096$, and $L \cong 4.2$. Curves h and s are dimensionless concentrations of *h* and *s*, respectively.

can be monostable or bistable even for so simple a system as that represented by Eqs. **3**–**5**.

Experimentally, we find that our system exhibits bistability in the CFUR. For the same reactant concentrations in the feeding chamber, the entire gel with immobilized GO can be at a high pH (and high [$F_i$] with dark color) or a low pH (and low [$F_i$] with light color), depending on the initial conditions in the gel. We performed experiments on the stability of two coexisting steady states (SSs) separated by a front, which in general can move or remain stationary. Fig. 3*a* shows a snapshot of two approaching fronts separating the high pH SS in the center from two identical low pH SSs initiated at either end of the medium. The fronts are not stable; they approach one another and collide in the middle, so that the entire medium becomes white. For a broad range of concentrations that support bistability, we found that a front between two SSs always moves into the high pH SS. Approaching fronts always collide, obliterating the high pH SS.

Fig. 3*b* is a snapshot illustrating enzyme immobilization on a restricted domain. In this case, GO has been immobilized in an annular region that allows propagation of a quasi-1D front in the 2D gel. Initiation of the low pH SS in a small area resulted in two fronts traveling at the same speed in opposite directions around the annulus. After collision, the entire annular domain with immobilized GO remained in the low pH SS.

**Experimental Pulses.** After finding propagating fronts, we next sought to create propagating pulses. A propagating pulse in a spatially extended system should be related to excitability in a point (0D) or well stirred system, where a superthreshold perturbation results in a large amplitude excursion before the system returns to its initial stable SS. Many models possessing pH bistability and oscillations also exhibit excitability (29–31). The region of excitability is often located near the Hopf bifurcation that leads to oscillations or near the saddle-node bifurcation that results in bistability (32, 33). Our first task was thus to locate the boundary between the bistable region and the high pH SS (SSI), where excitability is possible.

The GO–G–$F_i$ system has only one stable SS, namely SSII, the low pH equilibrium state, under batch conditions. In a CSTR, the system exhibits both the stable SSII and SSI as well as bistability between these SSs. As mentioned above, spatial bistabilty occurs in the CFUR. We were not, however, able to obtain SSI in the CFUR, because doing so requires a very thin gel layer (analogous to a very short residence time in the CSTR), in which the patterns become invisible. Therefore, some back reaction, like Eq. **9**, is necessary to stabilize the high pH SSI to make excitability and pulse propagation possible.

Addition of $H_2O_2$, i.e., selecting Eq. **9** as the back reaction, proved to be a good choice, because the GO–G–$F_i$–$H_2O_2$ system can be quasibistable, even under batch conditions. For example, at [GO] = 0.3 mg/ml, [$F_i$] = 10 mM, [G] = 25 mM, and [$H_2O_2$] = 20 mM, two different states with pH $\cong$ 3 and pH $\cong$ 7 (obtained with initial pH values of 5 and 9, respectively) were maintained for >1 h.

By varying [$H_2O_2$] in CFUR experiments, we obtained propagating fronts similar to the one shown in Fig. 3*a* at low [$H_2O_2$], propagating pulses at higher [$H_2O_2$] (Fig. 3*c*), and damped propagating pulses at still higher [$H_2O_2$]. A space–time plot for this last experiment is shown in Fig. 4*c*. Space–time plots for a front and a pulse shown in Fig. 4 *a* and *b*, respectively, demonstrate that both fronts and pulses propagate with constant velocity. Comparing these velocities with the data shown in Fig. 2, we see that $H_2O_2$ decelerates front/pulse propagation.

Experiments in an annular domain were performed to study the interaction between pulses. After an initial perturbation, two

pulses propagate around the ring with identical velocity and annihilate on collision, as in the case of interacting fronts (Fig. 3*b*), except that here the annular ring remains dark (SSI) after the collision.

In an attempt to obtain a single continuously rotating pulse on the annular ring, we suppressed one of the two initial pulses by briefly subjecting it to intense illumination (34, 35). The remaining single pulse is shown in Fig. 3*d*. Unfortunately, the pulse died out as soon as it reached the previously illuminated region, probably because the illumination reduced the activity of GO. Lower intensity illumination failed to suppress the pulse.

**Simulations of Front Propagation in Batch Experiments.** Comparing our experimental results with Eq. **1**, we find two significant discrepancies. First (Fig. 2*a*), the front velocity approaches zero at positive $s_0$. Second (curve 1 of Fig. 2*c*), the constant $k'_{ox}$ in Eq. **8** is not independent of $[H^+]$ but ranges between $k_1$ and $k_2$. It is not clear which of these values, or what combination of the two, is appropriate to use in the rate constant $k$ in Eq. **1**.

To address these questions, we supplemented Eqs. **3–5** with two protonation-deprotonation reactions (14):

$$\mathrm{PGOH} \leftrightarrow \mathrm{PGO} + \mathrm{H}^+ \quad K_G \qquad [10]$$

and

$$\mathrm{F_eH} \leftrightarrow \mathrm{F_e} + \mathrm{H}^+ \quad K_F, \qquad [11]$$

where PGO represents an average protonatable GO residue, the total number of which is $N_{AG}$ ($\cong$200) per protein globule of GO. $K_G$ and $K_F$ are equilibrium constants that are related to the corresponding forward and reverse reaction rate constants as $k_{ff} = k_b K_F$, $k_{fg} = k_b K_G$; $k_b = 10^9$-$10^{10}$ $M^{-1}\cdot s^{-1}$ (diffusion-controlled bimolecular reaction rate constant for protonation reactions). Eqs. **3–5** and **10** and **11** give rise to the following partial differential equations (PDEs):

$$\partial h/\partial t = 2v_e - k_b p h + k_{ff} p_h - k_b[\mathrm{PGO}]h + k_{fg} (N_{AG} e_t - [\mathrm{PGO}]) + D_h \Delta h, \qquad [12]$$

$$\partial s/\partial t = -2v_e + D_s \Delta s, \qquad [13]$$

$$\partial p/\partial t = 2v_e - k_b p h + k_{ff} p_h + D_p \Delta p, \qquad [14]$$

$$\partial p_h/\partial t = k_b p h - k_{ff} p_h + D_{ph} \Delta p_h, \qquad [15]$$

and

$$\partial[\mathrm{PGO}]/\partial t = -k_b[\mathrm{PGO}]h + k_{fg}(N_{AG} e_t - [\mathrm{PGO}]), \qquad [16]$$

where $v_e$ is determined by Eq. **6**, $[H^+] \equiv h$, $[F_e] \equiv p$, $[F_eH] \equiv p_h$, $N_{AG}e_t - [\mathrm{PGO}] = [\mathrm{PGOH}]$, $\Delta$ is the Laplacian operator (in our 1D simulations, $\Delta = \partial^2/\partial x^2$, where $x$ is the spatial coordinate), and $D_i$ is the diffusion coefficient of species $i$. Eqs. **12–16** describe batch experiments of the type shown in Fig. 1.

The results of simulations using these equations with zero-flux boundary conditions are shown in Fig. 2 *b–d*. We made the plausible assumption that $D_h > D_s = D_p = D_{ph}$ and used reaction rate constants obtained (14) in a CSTR. Fig. 2*b* shows that the front velocity $v$ tends to zero at nonzero $s_0$ in this model [$v = 0$ at $s_0 = 0.1 \times 10^{-4}$ M (curve 1), $1.53 \times 10^{-4}$ M (curve 2), and $3.75 \times 10^{-4}$ M (curve 3)]. These values of $s_0$ (which we dub $s_{0\text{-}0}$) increase with $e_t$. These results suggest that the buffering property of the enzyme, i.e., Eq. **10**, which removes free protons from solution, is responsible for the nonzero values of $s_{0\text{-}0}$. At larger $e_t$, curve 2 in Fig. 2*c* tends to a plateau, also as a result of Eq. **10**, which slows the autocatalytic production of $h$. The buffering properties of the enzyme have been discussed in detail elsewhere (30). The dependence of $v$ on $D_h$ in Fig. 2*d* demonstrates that $v \neq 0$ at $D_h = 0$, in contradiction to Eq. **1**. We attribute this behavior to the protonation reaction, Eq. **11**. Bound protons can diffuse in the form of $F_eH$.

The slopes of the theoretical curves can shed light on the appropriate choice of the constant $k$ in Eq. **1**, although we already know that Eq. **1** does not provide a complete description of the system because of the presence of Eqs. **10** and **11**. However, in certain limiting cases, e.g., when $D_h \gg D_s = D_p = D_{ph}$ and $e_t$ is small, this equation is still valid, because $v \propto (s_0 e_t D_h)^{1/2}$. The coefficient of proportionality between $v$ and $(s_0 e_t D_h)^{1/2}$ can be extracted from the slopes of the theoretical curves (=0.009 $cm\cdot s^{-1}\cdot M^{-1/2}$ for curve 1 in Fig. 2*b*, 4.1 $cm\cdot s^{-1}\cdot M^{-1/2}$ for curve 2 in Fig. 2*c*, and 0.153 $s^{-1/2}$ for Fig. 2*d*). We find that $v = 2(k s_0 e_t D_h)^{1/2}$ with $k = (1.2\text{–}1.4) \times 10^7$ $M^{-2}\cdot s^{-1}$, which is slightly above $(k_1 k_2)^{1/2}$. Assuming that the rate constants in the gel are the same as in aqueous solution and that $k'_{ox} \equiv k = (1.2\text{–}1.4) \times 10^7$ $M^{-2}\cdot s^{-1}$, we can estimate $D_h$ from our experimental results [$2(D_h k'_{ox})^{1/2} = 12\text{–}16$ $cm\cdot s^{-1}\cdot M^{-1}$] as $D_h \cong 4 \times 10^{-6}$ $cm^2\cdot s^{-1}$. This value is surprisingly small, which we attribute to the fact that $k_1$ and $k_2$ (see Eq. **7**) for the enzymatic reaction in a gel are several times smaller than in aqueous solution. Determining $D_h$ more accurately will require further kinetic experiments with GO immobilized in a gel to find the correct values of $k_1$, $k_2$, and $K_e$ for autocatalysis (see Eq. **7**).

**Simulations of Pulse Propagation.** To explore the parameter regime in which excitability and pulse propagation can arise in our system, we must supplement the PDEs Eqs. **12–16** with additional terms arising from Eq. **9** and add a new variable, $[H_2O_2]$. The resulting equations are given in *SI Results*. Here, instead, we consider a more general "activator-depleted substrate" model of pulse propagation. We analyze the following set of equations (30).

$$\partial h/\partial t = sh + F(h) - \alpha h + D_h \Delta h \qquad [17]$$

and

$$\partial s/\partial t = -sh - \alpha(s-1) + D_s \Delta s, \qquad [18]$$

where $F(h) = \beta/(\gamma + h) - \alpha R$ or $F(h) = \alpha\varepsilon - bh/(\gamma + h)$; i.e., $F(h)$ is a sigmoidal function of $h$ that changes significantly at $h \sim \gamma$ and $F(h) = C_1 < 0$ at $h \gg \gamma$ and $F(h) = C_2 > 0$ at $h \ll \gamma$ ($h \ll \alpha\varepsilon/b < 1$). The term $F(h)$ is analogous to our feedback reaction, Eq. **9**. $sh$ represents autocatalysis, $-\alpha h$ and $-\alpha s$ are outflow terms, and $\alpha$ is a constant inflow rate for the substrate $s$. The system represented by Eqs. **17** and **18** gives both bistable and oscillatory behavior. We performed simulations only for parameters close to the bistability region because, in our experimental system, we found only bistability. Zero-flux boundary conditions were used.

To be more specific, we consider the system represented in Eqs. **17** and **18** with $F(h) = \beta/(\gamma + h) - \alpha R$, where $R = [OH^-]_0/[S]_0$ and $[OH^-]_0$ and $[S]_0$ are the input concentrations of hydroxyl ions and substrate; the dimensionless variables $h$ and $s$ are equal to $[H^+]/[S]_0$ and $[S]/[S]_0$, respectively; and $\alpha$ is proportional to $k_0/[S]_0$, where $k_0^{-1}$ is the "residence time" in the reactive layer (characteristic time for diffusion through the layer). If either $\alpha$ or $R$ is increased, the 0D system of Eqs. **17** and **18** (without diffusion terms) passes from the low pH monostable SS (SSII) to the bistable state (BS) and then to the monostable high pH state (SSI). Near the boundary between BS and SSI, SSI is excitable. Upon adding diffusion terms, we find pulse solutions. Fig. 4*d* demonstrates such a pulse in 1D that has an almost rectangular shape with length $L$. This length is given by the simple expression $L \cong v\tau$, where $v$ is the velocity of the pulse and $\tau$ is the characteristic time for the 0D system to return to the initial stable SS after a superthreshold perturbation. The shape of this "excursion kinetics" in time mirrors that of the pulse in

space (the space axis in Fig. 4*d* can be replaced by an oppositely directed time axis). For example, for the parameters shown in Fig. 4*d*, $\tau \cong 440$, and $L \cong v\tau = 4.2$. Note that, when Eq. **9** provides the negative feedback, an increase in the parameter $R$ is equivalent to an increase in $[H_2O_2]$. Simulations also reveal that, if we are too far from the BS/SSI boundary, we find only propagating fronts in the BS domain or damped pulses in the SSI domain. These theoretical results correspond well to our experimental findings.

**Discussion and Conclusion.** Propagating fronts and pulses are well known dynamical patterns, but the fronts and pulses presented in this work are examples of such patterns in a simple (and inexpensive) enzymatic reaction. To obtain a pulse, a back reaction was required. We selected Eq. **9**, but this reaction can be replaced with a second proton-consuming enzymatic reaction. The second enzyme can be immobilized in another, coupled, gel layer, which could open up a variety of routes to obtaining complex patterns in spatially extended enzymatic systems.

The activity of an enzyme, in general, can be modulated by various small molecules, activators, and inhibitors. This feature distinguishes biological catalysts, i.e., enzymes, from inorganic catalysts. For example, the activity of GO depends on $[Cl^-]$ at pH 3–5, on micromolar amounts of heavy metals, and on the concentrations of substrates and products (17). Exploiting these features may allow us finer control over front and wave velocities in future experiments.

Our experimental results are in qualitative agreement with the predictions of our proposed mechanism, although the rate constants of the enzymatic reaction will need to be adjusted to immobilized enzyme conditions. The pulse shape (Fig. 4*d*) predicted by the very simple model represented by Eqs. **17** and **18** resembles strongly the shape of the pulse found in our experiments (Fig. 3*d* or horizontal cross-section of Fig. 4*b*). However, the full mechanism of this system is undoubtedly more complex. We have neglected, for example, inhibition of GO by $F_i$ at low pH (14) as well as other fine details.

## Materials and Methods

The reagents used were GO from *A. niger* (Fluka, Seelze, Germany), potassium $F_i$ [$K_3Fe(CN)_6$; Fluka], sodium hydroxide (NaOH; Fisher Scientific, Waltham, MA), sulfuric acid ($H_2SO_4$; Fisher Scientific), D(+)-G anhydrous (Fluka), and hydrogen peroxide ($H_2O_2$; Fisher Scientific). To calculate the molar concentration of enzyme, $e_t$, from the measured value in milligrams per milliliter, we used a molecular weight for a two-subunit GO of 155,000 (15, 17).

All experiments were carried out in a 0.3-mm-thick polyacrylamide gel (18% acrylamide, catalog no. A3449; Sigma, St. Louis, MO). GO was physically immobilized in the gel by mixing with an acrylamide/bis-acrylamide mixture before polymerization. After polymerization, the GO-containing gel was washed with distilled water. Next, the gel was immersed for 10 min in a solution containing 100 mM G, 0–50 mM hydrogen peroxide, and 2.5–25 mM $F_i$ brought to pH 10 by addition of NaOH. At this pH, the autocatalytic reaction is extremely slow, with rapid autocatalysis beginning only after $\approx$1 h, which allowed us to manipulate the reactive gel before initiating the front. Finally, the gel was wiped to remove any excess chemicals from its surface.

For experiments in quasi-1D domains, a long, narrow slice of gel was quickly placed between two flat optical windows in such a way that a short (<5 mm) portion of the slice protruded beyond the windows (see Fig. 1). The optical windows protected the gel from drying and restricted access of oxygen to the gel. The protruding end of the slice was used for initiation of the front. We prepared a small piece of the same gel immersed in the same solution of G and $F_i$ but at pH 3 due to addition of $H_2SO_4$. Simply touching the open end of the long gel slice with the piece of acidic gel initiated the autocatalysis and front propagation.

For experiments in 2D domains, we used an open system, a CFUR. A continuously stirred feeding chamber with a volume of 50 ml was separated from the gel layer by a rigid Anapore membrane (catalog no. 6809-5022; Whatman, Florham Park, NJ) and a nitrocellulose membrane (catalog no. GSTF04700; Millipore, Billerica, MA), both with diameters of 50 mm. The feeding chamber was filled with the reactants (G, $F_i$, and NaOH as well as $H_2O_2$ when required), which diffused into the gel through the membranes. The volume of the feeding chamber (50 ml) is 65 times the volume of the gel, which implies that the residence time in the chamber plays essentially no role in determining the behavior in the gel.

For observation and recording purposes, the gel was illuminated with low-intensity white light through an optical window. Reflected light was recorded by a CCD camera using a 420-nm interference filter for all experiments (the maximum light absorption by $F_i$ occurs close to this wavelength). In this way, we were able to track changes in the $F_i$ concentration: dark for high concentration and light for low concentration.

The fact that GO can be immobilized in the gel allows us to perform experiments with different geometrical configurations. The gel was fashioned in striped or annular segments depending on the experimental requirements. To accomplish this variety of configurations, we prepared two solutions for polymerization but only one containing GO. Then the enzyme-containing solution was polymerized and cut into the desired shape. Next, the enzyme-free solution of acrylamide was poured over the previous gel and polymerized so that the original piece of gel was incorporated into the new one. In this way we created gels with homogenous physical characteristics but with the enzyme immobilized in only part of the gel. This technique allowed us to observe 1D fronts and pulses in a 2D gel and to perform experiments where waves propagated along a predesigned path as well as 1D experiments on closed loops.

PDEs were solved numerically in 1D with the FlexPDE package (PDE Solutions, Sunol, CA), in which a Newton–Raphson iteration process is used with a variable time step and mesh. FlexPDE refines the triangular finite element mesh and/or time step until the estimated error in any variable is less than a specified tolerance, which we chose as $5 \times 10^{-8}$ for the PDEs Eqs. **12–16** and $2 \times 10^{-6}$ for PDEs Eqs. **17** and **18** (see below) at every cell of the mesh.

This work was supported by Chemistry Division of the National Science Foundation Grant CHE-0615507.

1. Keener J, Sneyd J (2004) *Mathematical Physiology* (Springer, New York).
2. Lechleiter J, Girard S, Peralta E, Clapham D (1991) *Science* 252:123–126.
3. Mair T, Müller SC (1996) *J Biol Chem* 271:627–630.
4. Mair T, Warnke C, Müller SC (2001) *Faraday Discuss* 120:249–259.
5. Kindzelskii AL, Petty HR (2002) *Proc Nat Acad Sci USA* 99:9207–9212.
6. Petty HR, Kindzelskii AL (2001) *Proc Nat Acad Sci USA* 98:3145–3149.
7. Zaikin AN, Zhabotinsky AM (1970) *Nature* 225:535.
8. Fisher RA (1937) *Ann Eugen* 7:355–369.
9. Kolmogorov AN, Petrovski IG, Piskunov NS (1937) *Bull Moscow State Univ Ser A* 1:1–25.
10. Vanag VK, Epstein IR (2003) *Proc Natl Acad Sci USA* 100:14635–14638.
11. Epstein IR, Vanag VK (2003) In *Experimental Chaos: Seventh Experimental Chaos Conference*, eds Kocarev L, Carroll TL, Gluckman BJ, Boccaletti S, Kurths J (Am Inst of Phys, Melville, New York), pp 265–274.
12. Lee KJ, McCormick WD, Ouyang Q, Swinney HL (1993) *Science* 261:192–194.
13. Lee KJ, McCormick WD, Pearson JE, Swinney HL (1994) *Nature* 369:215–218.
14. Vanag VK, Míguez DG, Epstein IR (2006) *J Chem Phys* 125:194515.
15. Leskovac V, Trivic S, Wohlfahrt G, Kandrac J, Pericin D (2005) *Int J Biochem Cell Biol* 37:731–750.
16. Weibel MK, Bright HJ (1971) *J Biol Chem* 246:2734–2744.

17. Wilson R, Turner APF (1992) *Biosens Bioelectron* 7:165–185.
18. Takahashi T, Mitsumoto M (1963) *Nature* 199:765–767.
19. Wohlfahrt G, Trivic S, Zeremski J, Pericin D, Leskovac V (2004) *Mol Cell Biochem* 260:69–83.
20. Field RJ, Burger M (1985) *Oscillations and Traveling Waves in Chemical Systems* (Wiley, New York).
21. Epstein IR, Pojman JA (1998) *An Introduction to Nonlinear Chemical Dynamics* (Oxford Univ Press, New York).
22. Rábai G, Kustin K, Epstein IR (1989) *J Am Chem Soc* 111:3870–3874.
23. van Saarloos W (1988) *Phys Rev A* 37:211–229.
24. van Saarloos W (1989) *Phys Rev A* 39:6367–6390.
25. Horvath D, Petrov V, Scott SK, Showalter K (1993) *J Chem Phys* 98:6332–6343.
26. Vanag VK, Epstein IR (2002) *J Chem Phys* 117:8508–8514.
27. Szalai I, De Kepper P (2006) *Phys Chem Chem Phys* 8:1105–1110.
28. Blanchedeau P, Boissonade J, De Kepper P (2000) *Physica D* 147:283–299.
29. Vanag VK, Epstein IR (2005) *Phys Rev E* 71:066212.
30. Zagora J, Voslar M, Schreiberova L, Schreiber I (2001) *Faraday Discuss* 120:313–324.
31. Zagora J, Voslar M, Schreiberova L, Schreiber I (2002) *Phys Chem Chem Phys* 4:1284–1291.
32. McCormick WD, Noszticzius Z, Swinney HL (1991) *J Chem Phys* 94:2159–2167.
33. Voslar M, Schreiber I (2004) *Phys Rev E* 69:026210.
34. Kaminaga A, Rábai G, Mori Y, Hanazaki I (1996) *J Phys Chem* 100:9389–9394.
35. Kaminaga A, Rábai G, Hanazaki I (1998) *Chem Phys Lett* 284:109–114.